Experimental analysis of waveform effects on satellite and ligament behavior via *in situ* measurement of the drop-on-demand drop formation curve and the instantaneous jetting speed curve



2010 J. Micromech. Microeng. 20 115005

(http://iopscience.iop.org/0960-1317/20/11/115005)

IOP Publishing Journal of Micromechanics and Microengineering

J. Micromech. Microeng. **20** (2010) 115005 (14pp) doi:10.1088/0960-1317/20/11/115005

# Experimental analysis of waveform effects on satellite and ligament behavior via *in situ* measurement of the drop-on-demand drop formation curve and the instantaneous jetting speed curve

**Kye-Si Kwon**

Department of Mechanical Engineering, Soonchunhyang University, 646, Eupnae-ri, Shinchang-myeon, Asan-si, Chungcheongnam-do 336-745, Korea

E-mail: kskwon@sch.ac.kr

Received 27 April 2010, in final form 4 September 2010
Published 4 October 2010
Online at stacks.iop.org/JMM/20/115005

**Abstract**

*In situ* techniques to measure the drop-on-demand (DOD) drop formation curve and the instantaneous jetting speed curve are developed such that ligament behavior and satellite behavior of inkjet droplets can be analyzed effectively. It is known that the droplet jetting behavior differs by ink properties and the driving waveform voltage. In this study, to reduce possible droplet placement errors due to satellite drops or long ligaments during printing, waveform effects on drop formation are investigated based on the measured DOD drop formation curve and the instantaneous jetting speed curve. Experimental results show that a dwell time greater than the so-called efficient dwell time was effective in reducing placement errors due to satellite drops during the printing process.

(Some figures in this article are in colour only in the electronic version)

## 1. Introduction

Inkjet technology has been used in printed electronics applications such as large area displays, radio frequency identification (RFID) and printed circuit boards (PCB) [1–4]. As inkjet applications broaden, various types of jetting materials are required to be precisely dispensed from the inkjet head. Therefore, droplet behavior from the inkjet head must be well controlled and proper measurement of jetting performance is increasingly important. Measured jetting behavior can be used to improve jetting performance by modifying either the functional ink properties or the driving waveform voltage.

To evaluate jetting performance from inkjet dispensers, images from charge-coupled device (CCD) cameras are widely used to measure droplet speed as well as droplet volume [1, 5–7]. By using light-emitting diode (LED) lights synchronized to the firing signal, droplet images appear to be frozen in the acquired CCD camera image. Then, image processing techniques are used to measure ink droplet locations at two different timings for jetting speed measurement [5, 6]. Droplet volume can be calculated using the droplet diameter, which can be obtained from a droplet image assuming that the droplet shape is spherical [5]. However, as jetting speed increases, the inkjet droplet will not remain spherical in shape since it is likely to have ligaments as well as satellites. Recently, Hutchings *et al* have developed image processing techniques to obtain the volume of ink droplets with ligaments [7]. The sliced width of a ligament of a droplet image in the lateral direction was used for the measurement. However, this method might not be effective in measuring satellite break-up and merging behavior because it mainly analyzed the shape of droplet using the width of the ligament in the lateral direction rather than in the jetting direction.

 

Dong *et al* used the so-called drop-on-demand (DOD) drop formation curve to understand satellite and ligament behavior [8]. The DOD drop formation curve is a plot of droplet locations with respect to time. Later, DOD drop formation curves were used by Jang *et al* to investigate the effects of ink properties on printing quality [9]. However, significant effort was needed to obtain the DOD drop formation curve since the droplet locations are determined from many sequential images. Thus, *in situ* automatic measurement methods are required for practicality. To the author's knowledge, *in situ* measurement techniques for the DOD drop formation curve have not yet been reported in the literature. In this work, automatic measurement techniques for the curve are presented such that measurement and analysis can be done quickly during jetting. The proposed approach could allow an ink developer to gain quick physical insight of drop formation behavior in relation to ink properties and the driving voltage waveform.

In addition to ink properties, the inkjet waveform can significantly alter jetting behavior [10]. Previous studies considered the effect of ink properties on drop formation rather than the effect of the waveform [8–11]. However, without proper selection of the waveform, satellite behavior due to ink properties may be difficult to understand fully because ink jetting behavior results from the combined effect of both the waveform and the properties of the ink. Recently, Dong showed that satellite behavior could be changed by modifying the driving waveform [12]. However, the waveform used consisted of a long rising section and a short falling section, and did not have a dwell section. During the long rising time, a negative pressure wave of ink is generated inside the printhead. At the same time, the pressure wave propagates during the long rising time. As a result, it may be difficult to fully understand the correlation between the waveform and droplet behavior because the waveform effects from the long rising section have a mixed effect on pressure wave behavior. On the other hand, a simple trapezoidal waveform has been widely used in practice for controlling jetting behavior [13–15]. For this waveform, a fixed value for both the rising time and the falling time is used. Therefore, the waveform design issue is focused on determining the dwell time [13–15]. To find the proper dwell time, the relationship between the droplet jetting speed and the dwell time has been sought [13–15]. In most waveform design methods, an efficient dwell time is sought to maximize the jetting speed. However, the waveform for maximizing jetting speed is not always the optimal waveform in terms of printing quality. For example, the existence of satellites or ligaments during drop formation can result in placement errors during printing when the inkjet head or substrate is moving. In this study, the effect of the driving waveform on drop formation is analyzed to determine effective dwell time for suppressing satellite and ligament formation. For this purpose, the DOD drop formation curve was measured to understand jetting behavior in relation to waveform. In addition, we propose the use of an instantaneous jetting speed curve to determine the proper waveform to suppress satellites because the relative jetting speed of a satellite with respect to the main droplet can be understood during the entire drop formation. The instantaneous jetting speed curve is the plot of jetting speeds of droplets with respect to time. Here, the jetting speeds were measured during a short period such that the speed variations of all droplets during drop formation could be fully understood. Based on experimental results, a rule of thumb for determining the dwell time required to suppress satellite drops is proposed.

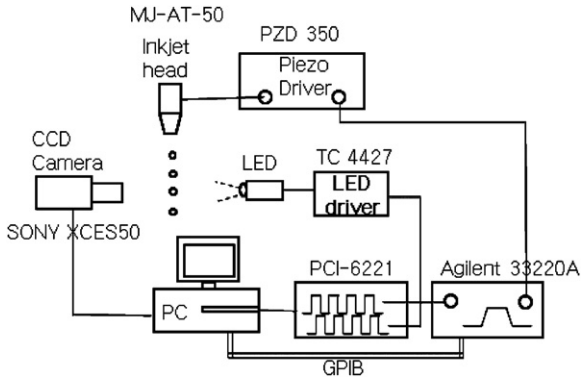


**Figure 1.** Experimental setup.

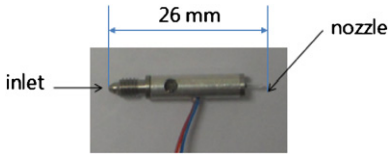


**Figure 2.** Inkjet head (Microfab, MJ-AT, USA).

If satellites or ligaments are unavoidable, the standoff distance (i.e. the distance between the nozzle surface and the substrate) must be adjusted to minimize placement errors. Jang *et al* showed that the optimal standoff distance in relation to ligament length was characterized only by ink material properties (i.e. the $Z$ number, which is the inverse of the Ohnesorge number) [9]. However, since the waveform can significantly affect drop formation, the optimal standoff distance may be difficult to generalize with respect to jetting fluids only. We propose the use of the equivalent droplet length in the jetting direction to determine the optimal standoff distance. This approach can minimize placement errors due to satellites or ligaments.

## 2. Jetting behavior measurement

In this study, the laboratory-developed drop watcher system shown in figure 1 was used to measure jetting speed and inkjet droplet formation behavior.

A single nozzle head (MJ-AT, Microfab, USA), shown in figure 2, was used as the jetting device. The nozzle diameter of the printhead used for the experiment was 50 $\mu$m. A CCD camera (Sony XC ES 50) was used for droplet image acquisition. An adjustable zoom lens (ML-Z07545, MORITEX) and a lens adaptor (ML-Z20, MORITEX) were used to acquire magnified images of the inkjet droplets.

Two digital pulses were generated such that the first digital pulse train was used as a triggering signal for jetting and the

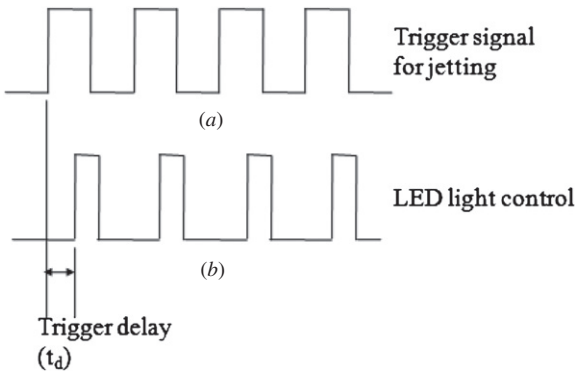


**Figure 3.** Digital pulse trains from two counters in PCI-6221.

second pulse was used to control the LED light. The ink jetting frequency was controlled by the first digital pulse train. Then, the second pulse was triggered from the first pulse. The trigger delay and the duty ratio of the second trigger were controlled. The duty ratio of the second pulse shown in figure 3(*b*) could change the image brightness by varying the light intensity of the LED. As a result of the synchronized LED light with respect to jetting, a droplet appears to be frozen in the acquired image.

To obtain sequential images, the trigger delay of the second digital pulse for the LED lights shown in figure 3(*b*) was controlled. For this purpose, the trigger delay $t_d$ of the second digital pulse with respect to the first digital pulse was increased from the user-defined starting time to the end time by predetermined steps throughout the time of interest. Using the LED light delay adjustment, sequential frozen images at each trigger delay time were obtained from the CCD camera. Each sequential image was then processed to extract inkjet drop information. A similar approach was used in the author's previous work to measure meniscus motion [15]. The images acquired from the CCD camera have 8-bit image pixels that can appear as gray with values ranging from 0 to 255 according to the brightness of the image as shown in figure 4(*a*). The gray image can be converted into a binary image in which the pixels have values of 0 or 1. The binary image can be obtained by setting an appropriate threshold value such that values higher than the threshold are mapped to 1 (or 0) and values lower than the threshold are mapped to 0 (or 1) as shown in figure 4(*b*). Using the converted binary image, ink droplet information can be extracted since the ink droplet's pixels have a value of 0 (or 1) and the background can be 1 (or 0).

To reduce the computational effort needed to perform binary image analysis, a rectangular-shaped region of interest (ROI) was used as shown in figure 4(*a*). Using the ROI, the processing time was reduced by analyzing part of the area rather than the total image area. In addition, ink droplet analysis was made easier because other structures in the image could be excluded in the analysis [5] as shown in figure 4(*b*).

The number of droplets including main droplet and satellites can be obtained from an analysis of binary images. In addition, the maximum and minimum locations of the $k_{\text{th}}$ droplet in the $y$ direction, denoted as $P_k^{\max}(t_d)$ and $P_k^{\min}(t_d)$, can be obtained as shown in figure 4(*b*). The superscripts 'max' and 'min' denote maximum and minimum locations, respectively. The DOD drop formation curve was updated by adding the calculated maximum and minimum locations of each droplet $P_k^{\max}(t_d)$ and $P_k^{\min}(t_d)$ in the graph before changing the trigger delay value $t_d$ for the next sequential image as shown in figure 4(*c*). Also, from the measured

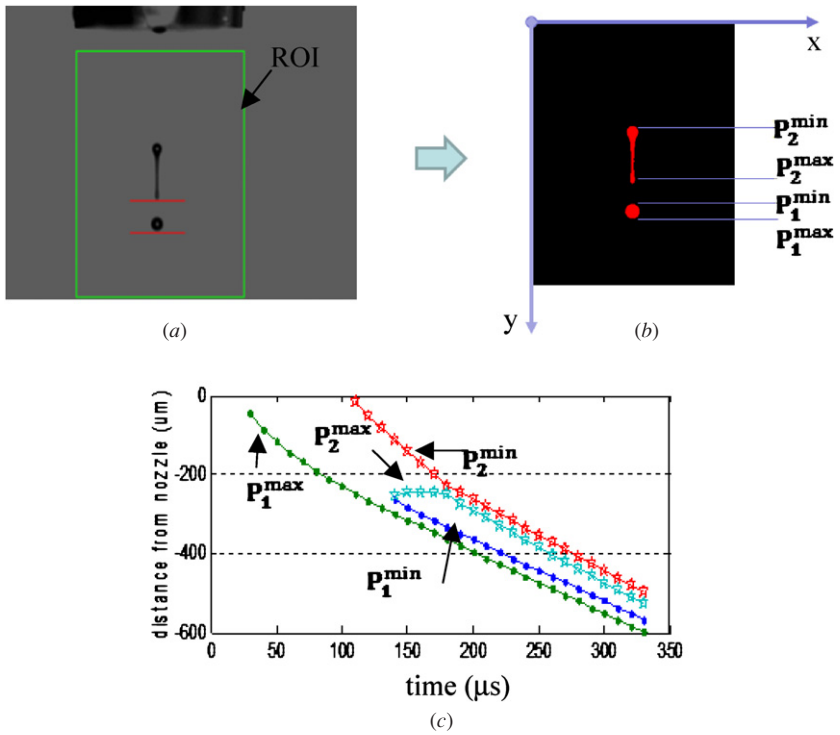


**Figure 4.** Image processing techniques for drop formation. (*a*) Droplet image, (*b*) binary image, (*c*) DOD drop formation curve.

locations of each droplet, the length of the ligament of the $k_{\text{th}}$ droplet $L_k(t_d)$ can be calculated as

$$L_k(t_d) = P_k^{\max}(t_d) - P_k^{\min}(t_d), \qquad k = 1, 2, \ldots, n \quad (1)$$

where $n$ is the number of droplets observed in the acquired CCD camera image. Also, the instantaneous jetting speeds of each droplet, $V_k^{\max}(t_d)$ and $V_k^{\min}(t_d)$ of the $k_{\text{th}}$ droplet were obtained as

$$V_k^{\max}(t_d) = \frac{\Delta(P_k^{\max}(t_d))}{\Delta(t_d)}, \qquad V_k^{\min}(t_d) = \frac{\Delta(P_k^{\min}(t_d))}{\Delta(t_d)}, \quad k = 1, 2, \ldots, n \quad (2)$$

where $\Delta(t_d)$ is the incremental time of trigger delay between the two consecutive images and $\Delta\left(P_k^{\max}(t_d)\right)$ and $\Delta\left(P_k^{\min}(t_d)\right)$ are the travel distance of the maximum and minimum location of the $k_{\text{th}}$ droplet during the time duration of $\Delta(t_d)$, respectively. We focused on the instantaneous jetting speeds of the maximum locations of ink droplets $\left(\text{i.e. } V_k^{\max}(t_d)\right)$ in this study. However, the actual droplet jetting speed of a droplet is difficult to define because the speed of the maximum locations in a droplet can differ significantly from the speed of the minimum location of the droplet if the droplet has a long ligament.

The existence of ligaments and satellites can significantly affect printing quality. Therefore, if these are unavoidable, a proper standoff distance, which can minimize these effects, should be determined. For this purpose, we define the equivalent droplet length, $L_{\text{eq}}(t_d)$, in the jetting direction as a function of time $t_d$ as follows:

$$L_{\text{eq}}(t_d) = P_1^{\max}(t_d) - P_n^{\min}(t_d). \quad (3)$$

Note that the equivalent droplet length is defined by the difference between the maximum location of the main (first) droplet and the minimum location of the last (final) drop. Placement error due to satellites or ligaments can be assessed using equation (3). Also, equation (3) can be used to determine the standoff distance for minimizing placement errors due to satellites or ligaments. The number of droplets $n$ is related to the number of satellites. In this study, we mainly considered a single droplet ($n = 1$) or two droplets ($n = 2$) for simplicity. The proposed method can be extended to the case of many satellite droplets ($n > 2$). However, the evaluation of jetting behavior of many satellite droplets may be difficult since $L_{\text{eq}}(t_d)$ in equation (3) is likely to become larger than the image size in the jetting direction. In this case, the proper measurement is impossible because some of the droplets would move out of the measured image range.

Since the droplet location is calculated from CCD camera images, measurement errors could occur due to the pixel resolution of the images. The image resolution of the camera system used in this experiment (XC ES 50, Sony) was 640 × 480. Zoom magnification can be used to reduce measurement errors. However, high magnification might not be effective for drop formation measurements since it could narrow the image view by focusing on a very small area, thereby making the overall drop formation difficult to understand. To evaluate this trade-off, we adjusted the zoom lens such that 1 pixel corresponded to about 1.4 $\mu$m, which resulted in a distance error of $\pm 0.7$ $\mu$m. A typical droplet size in the jetting direction ranged from about 50 to 200 $\mu$m depending on the ligament length, which corresponds to 36 to 143 image pixels. Therefore, the measured droplet error due to pixel resolution was about 0.7 to 2.8%. If the droplet volume is calculated from the droplet size, the errors should be reduced as much as possible because the droplet volume should be accurately measured for most applications. In this study, the droplet length (or size) information was used to determine the standoff distance to minimize placement error during printing. Thus, the errors of 3% due to pixel resolution may not be critical in this application. In addition to image resolution, there are binary conversion-related errors. The identified droplet sizes and locations in images can differ slightly depending on various conditions such as lighting brightness, lens focus and a threshold value for binary image conversion. Binary conversion errors affect the equivalent droplet length described in equations (1) and (3). Due to these binary conversion-related errors, the measurement error of identified droplet size can be up to 5% [5]. However, binary conversion errors are likely to be the same during the entire drop formation assuming that measuring conditions (lighting, lens focus, threshold value, etc) remain the same. Therefore, the measured jetting speed is less affected by binary conversion because the errors due to binary conversion could be cancelled out in the process of calculating the travel distance during the time duration. As a result, the instantaneous jetting speed is mainly affected by pixel resolution. If a time duration of 10 $\mu$s is used for the instantaneous jetting speed curves and the pixel resolution is 1.4 $\mu$m, the measurement errors of jetting speed due to the pixel errors can be 0.14 m s$^{-1}$. If we measure a jetting speed of 1 m s$^{-1}$, the measurement errors can be up to 14%. There are two methods for reducing jetting speed measurement errors. One method is to use a longer time duration between two consecutive images for the speed measurement. However, if the time duration is too long, then the speed variation is difficult to understand from the instantaneous jetting speed curve. The other method is to use a higher resolution camera, which may have cost issues. In this study, the relative jetting speed of the satellite with respect to the main droplet was mainly investigated to determine the proper waveform for suppressing satellites, which may not require precise measurement. Therefore, a jetting speed error of 10–20% may not be likely to change the conclusions or observations that were made in this study.

Figure 5 shows the menu of the developed software during measurement of the jetting behavior of ethylene glycol (EG). There is only a single droplet ($n = 1$) in this example. In most printing applications, the maximum location of a droplet $P_k^{\max}(t_d)$ is important in printing application since it is placed on the substrate first. Therefore, the behavior of the jetting speed at the maximum location $V_k^{\max}(t_d)$ rather than $V_k^{\min}(t_d)$ is discussed for an explanation of drop formation. Using the *in situ* measurement results shown in figure 5, the following analysis is possible during the jetting process.

(1) *Phase 1 (from 40 to 90 $\mu$s)*: A partial droplet is extruded from the nozzle. During the jetting process of phase 1, the instantaneous speed of the extruded part, $V_k^{\max}(t_d)$, is significantly reduced from 4.5 to 2.5 m s$^{-1}$. This effect

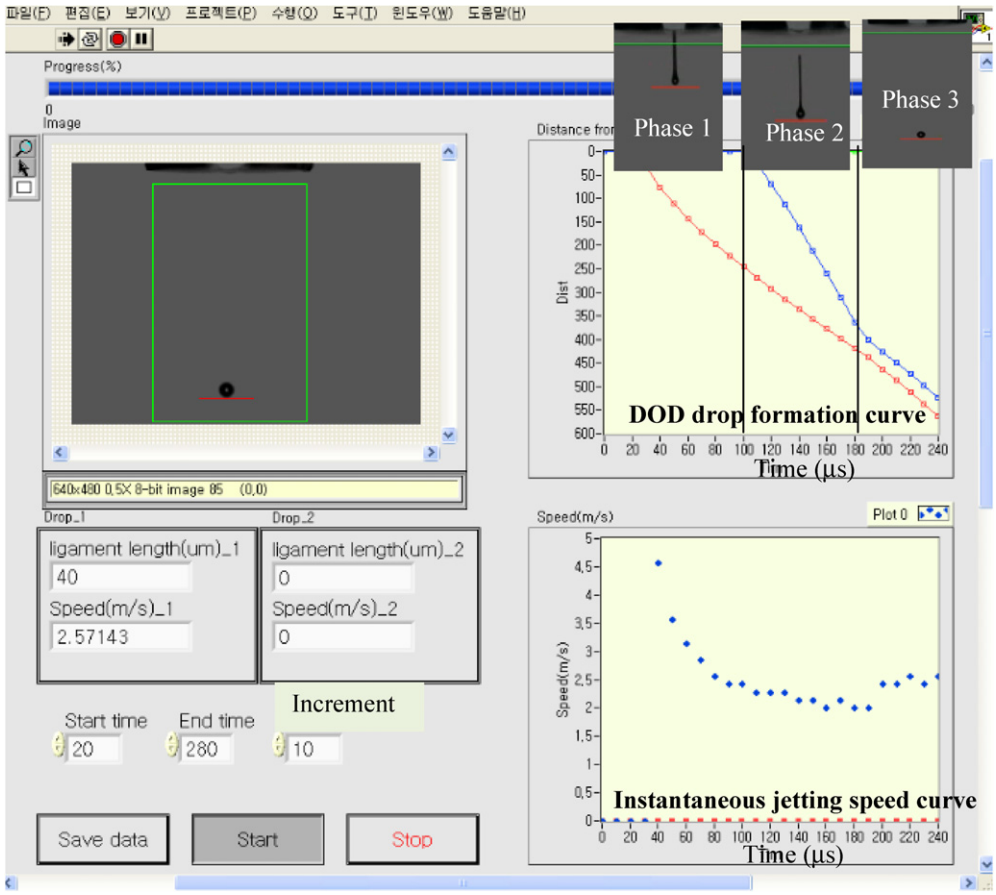


**Figure 5.** Software developed to measure drop formation.

may be due to the viscoelasticity of the fluids: the still-attached fluid at the nozzle may pull back the extruded fluid from the nozzle before the fluid is pinched off.

(2) *Phase 2 (from 90 to 180 μs)*: In phase 2, after pinch-off, the ink droplet drops in a condition of free-flying jetting, but still has a ligament. During phase 2, the instantaneous jetting speed of the leading end, $V_1^{\max}(t_d)$, was about 2 m $s^{-1}$. The jetting speed variation in the free-flying condition was small compared to the jetting speed variation in phase 1. Note that the ligament length was reduced because the speed of the tail end, $V_1^{\min}(t_d)$, was faster than $V_1^{\max}(t_d)$.

(3) *Phase 3 (from 180 μs)*: Finally, the lengthy ligament reconciles with the leading end of the droplet, resulting in a spherical droplet. During the reconciliation, the faster tail end (or minimum location) will increase the final jetting speed of the droplet from 2 to 2.5 m $s^{-1}$ as shown in figure 5. We note that the final jetting speed became almost constant (about 2.5 m $s^{-1}$) only after the shape of the droplet became spherical. Thus, when measuring the jetting speed by the conventional method using two different timings, it was required to measure the speed when the droplet became spherical. Otherwise, the measured speed may not represent the jetting performance since the measured jetting speed can be different according to the selection of the two timings.

Using the developed software algorithm, the jetting behavior could be understood during jetting. Here, the time-consuming effort of postprocessing numerous sequential images was not required to gain physical insight into droplet formation. The measured DOD drop formation data and instantaneous jetting speed data were saved on a computer hard disk for further analysis.

The proposed algorithm can be implemented in any drop watcher systems. There is a drop watcher module to measure jetting speed and droplet volume in most printing systems for printed electronics applications [1]. Thus, no additional cost is required to implement the proposed algorithm in an existing system.

## 3. Waveform effects on satellite droplets

For high quality printing, the satellite drop and ligament of an ink droplet must be suppressed during the jetting process. There are two methods to control inkjet drop formation. One method is to modify the jetting material properties such as surface tension and viscosity. The other method is to modify waveform voltages for the driving inkjet head. We characterized the waveform effects on drop formation by measuring the DOD drop formation and the instantaneous jetting speed curve. To compare the jetting behavior for different jetting material properties, fluid mixtures of EG and isopropyl alcohol (IPA) were used as shown

**Table 1.** Measured jetting fluid properties.

| | Jetting fluids (volume fraction) | Density (kg m$^{-3}$) | Surface tension (mN m$^{-1}$) | Viscosity (mPa s) | $Z$ number |
|---|---|---|---|---|---|
| 1 | Ethylene glycol | 1155 | 47.01 | 15.8 | 3.30 |
| 2 | Ethylene glycol (0.75) + isopropyl alcohol (0.25) | 1032 | 26.59 | 9.3 | 3.98 |
| 3 | Ethylene glycol (0.5) + isopropyl alcohol (0.5) | 975 | 25.144 | 7.68 | 4.56 |
| 4 | Ethylene glycol (0.25) + isopropyl alcohol (0.75) | 865 | 22.479 | 4.45 | 7.01 |
| 5 | Isopropyl alcohol | 797 | 20.344 | 2.17 | 13.12 |

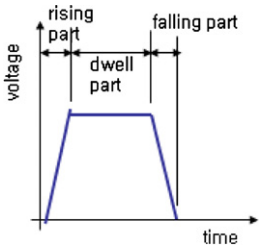


**Figure 6.** A typical trapezoidal waveform.

in table 1. To investigate the effects of jetting material parameters, viscosity and surface tension were measured using a Brookfield rheometer (VDV-III with UL adaptor) and a tensiometer (DST20, SEO), respectively. The temperature at which the material properties were measured was 22 °C (room temperature), and the jetting experiment was performed under the same temperature conditions. It is known that jetting phenomena can be characterized by the inverse ($Z$) of the Ohnesorge number (Oh), which is defined as follows [9, 11]:

$$Z = \frac{(a\rho\gamma)^{1/2}}{\eta}, \tag{4}$$

where $\rho$, $\gamma$, $\eta$ and $a$ are the density, surface tension and viscosity of the fluid and the radius of the nozzle orifice, respectively. It is known that a higher $Z$ value results in a more pronounced satellite in the jetted droplet [9, 11]. Thus, IPA will have a more pronounced satellite in the jetted ink droplet, whereas a ligament will be more developed in EG.

To control jetting performance from the inkjet head, the typical waveform shown in figure 6 was used. The parameters of the waveform shown in figure 6 must be properly determined to obtain the target jetting performance. Waveform design methods and the effect of each parameter were discussed in the author's previous work [15]. Dwell time is a critical parameter, and the most common method for understanding jetting performance with respect to the waveform uses the dwell time and jetting speed relationship [13–16].

Figure 7 shows the measured dwell time and jetting speed relationship of mixed fluids of EG and IPA from which the efficient dwell time of each material, which maximizes the jetting speed, can be determined. We note that the characteristics of jetting speed and the dwell time relationship were affected by jetting materials and the magnitude of input voltage, as shown in figure 7. The figure shows that as the $Z$ value increased, the decrease in jetting speed from the peak jetting speed became non-monotonic with respect to dwell time. This non-monotonic behavior of jetting speed resulted from different drop formation behavior according to the dwell time. The existence of satellites and ligaments during drop formation can significantly alter jetting speed. Thus, without understanding the effects of drop formation on jetting speed, it may be difficult to extract proper information from jetting speed and the dwell time relationship shown in figure 7. To measure jetting speed, most previous methods used two frozen droplet images at two different trigger delays $t_d$ in figure 2($b$) [5, 6]. However, a jetting speed measurement using two different timings may not represent the true jetting speed of a droplet since the speed varies significantly during the jetting process. As a result, the dwell time, which can result in maximum jetting speed, was changed when the voltage increased, as shown in figures 7($c$) and ($d$). Therefore, it is difficult to determine the efficient dwell time when the magnitude of the input voltage is high. An increase in the magnitude of the voltage can lead to increased jetting speed such that the satellite and ligament behavior affect drop formation significantly. Therefore, to determine the efficient dwell time, a dwell time and jetting speed relationship using low voltage was used in this study.

Figure 8 shows jetting images of fluid mixtures according to dwell times. The efficient dwell time can be understood by considering the travel distance of the droplet. For example, figure 8($b$) shows that a dwell time of 20 $\mu$s is close to the efficient dwell time for a fluid mixture of EG (0.75) and IPA (0.25), since the travel distance of the main droplet at 250 $\mu$s was longest. In addition, from the jetting images in figure 8, we note that dwell time affects both the jetting speed and the satellite behavior. However, it was difficult to fully understand drop formation behavior from the jetting images only. Thus, to understand drop formation and analyze the jetting speed variation during drop formation, we used the DOD drop formation curve and instantaneous jetting speed curve. Based on the measured curves, we also considered the effect of dwell time on the drop formation of a mixture of EG and IPA.

### *3.1. DOD drop formation curve and instantaneous jetting speed curve*

To investigate the dwell time effect on drop formation, two dwell times for each mixed fluid in table 1 were chosen such that one of the dwell times is shorter and the other is longer than the efficient dwell time of each jetting fluid. The two dwell times were selected from figure 7 such that the two jetting speeds of the main droplet (from the two dwell times) can be similar when the same magnitude of the voltage is used. The selection of a dwell time that results in similar jetting speed is important in investigating waveform effects, since it

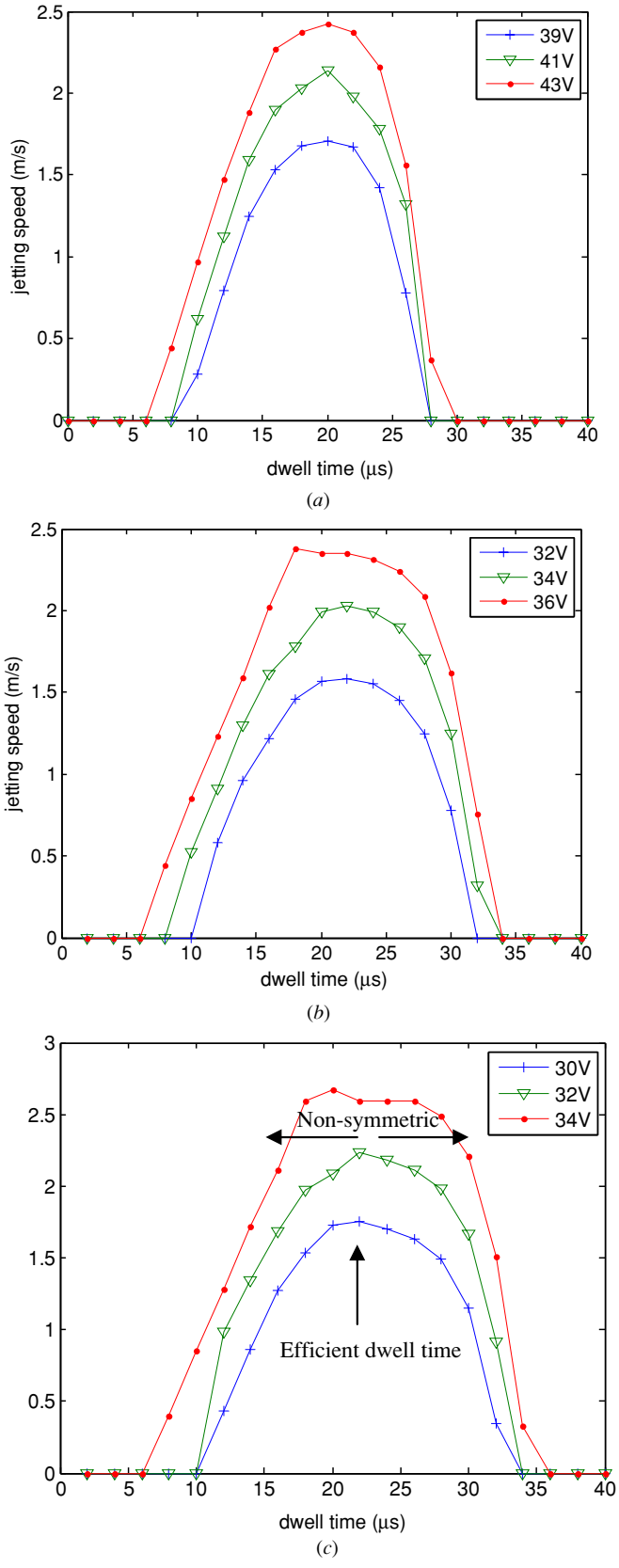


**Figure 7.** Jetting speed and dwell time relationship (rising time: 6 $\mu$s, falling time: 6 $\mu$s). (*a*) EG, $Z = 3.3$, (*b*) mixture of EG (0.75) and IPA (0.25), $Z = 3.98$, (*c*) mixture of EG (0.5) and IPA (0.5), $Z = 4.56$, (*d*) mixture of EG (0.25) and IPA (0.75), $Z = 7.01$ (*e*) IPA, $Z = 13.12$.

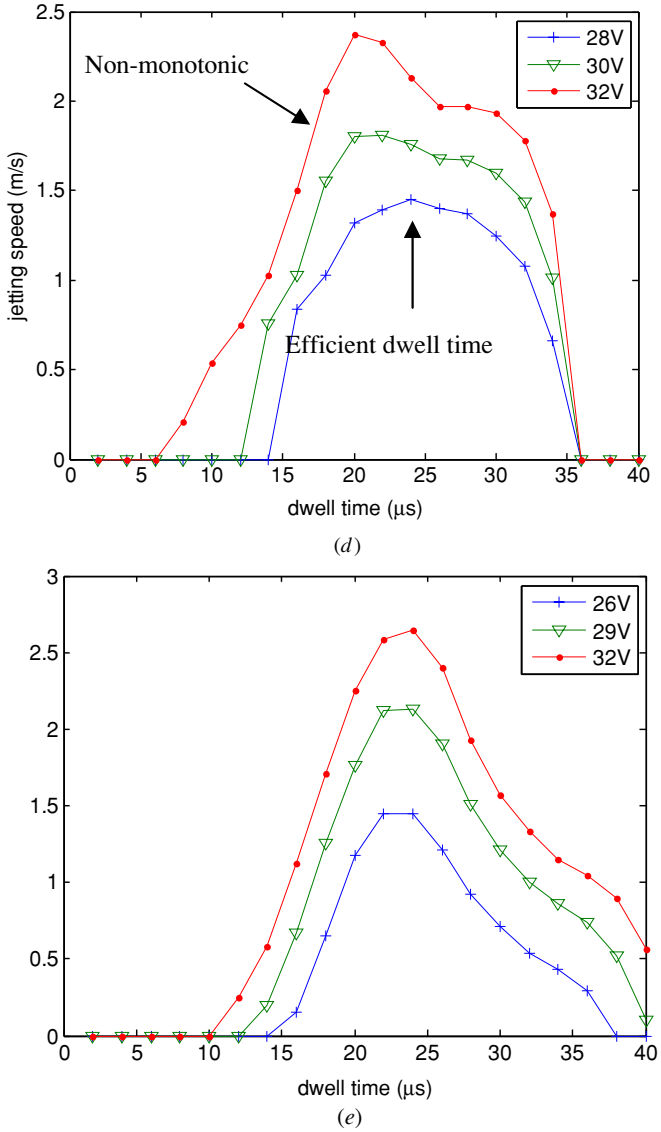


**Figure 7.** (Continued.)

is difficult to compare drop formation behavior with respect to waveform when the jetting speed is different. Note that a different jetting speed may result in different drop formation behavior including satellite and ligament.

Figures 9–13 compare the DOD drop formation curves with respect to two dwell times. From the curves, the pinch-off and breakup behavior of the jetted droplet can be clearly seen. In addition, satellite behavior can be investigated. The figures show that the $Z$ value of the fluids affects drop formation. For example, the ligament is more likely to break up into a main droplet and satellites, and the distance between the main droplet and the satellites becomes wider in the case of mixed fluids with more IPA than EG. Note that this satellite and ligament behavior can be suppressed significantly with a longer dwell time as shown in figures 10(*d*), 11(*d*), 12(*d*) and 13(*d*) This can be clearly understood from the comparison with jetting behavior using shorter dwell time as shown in figures 10(*a*), 11(*a*), 12(*a*) and 13(*a*). This indicates that the dwell time in the waveform can be a critical factor in drop formation.

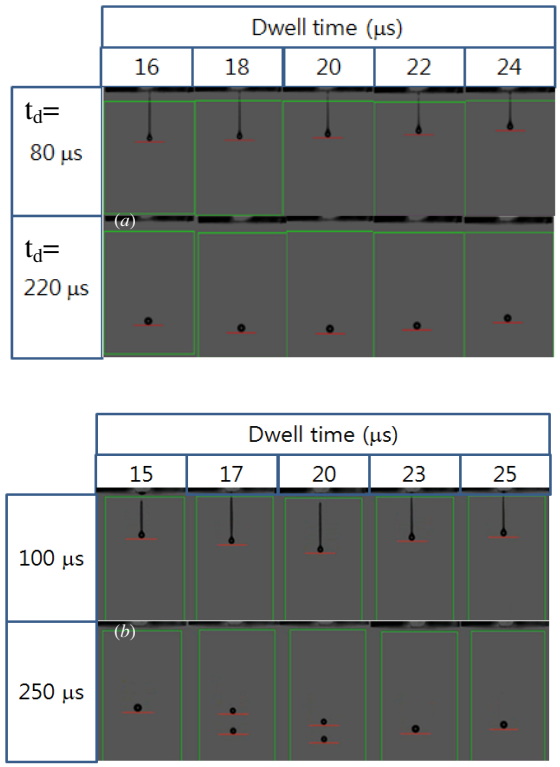


**Figure 8.** Droplet image in relation to dwell time and jetting fluids (rising/falling time: 6 $\mu$s). (*a*) EG, 41 V, (*b*) mixture of EG (0.75) and IPA (0.25), 34 V, (*c*) mixture of EG (0.5) and IPA (0.5), 32 V, (*d*) mixture of EG (0.25) and IPA (0.75), 32 V (*e*) IPA, 29 V.

We observed from the experiment that the satellite suppression via the waveform is related to the relative jetting speed of the satellite (the second droplet) with respect to the main droplet (the first droplet). If the jetting speed of the satellite (second droplet) is higher than the main droplet, the satellite droplet will eventually merge into the main droplet. If not, the distance between the main droplet and the satellite will become wider as the droplets travel. Therefore, a proper jetting speed measurement is essential to understanding the relative jetting speed of the satellite with respect to the main droplet. However, the conventional jetting speed measurement has drawbacks when used to analyze this jetting behavior during drop formation. First, the measured jetting speed using the conventional method may give misleading information

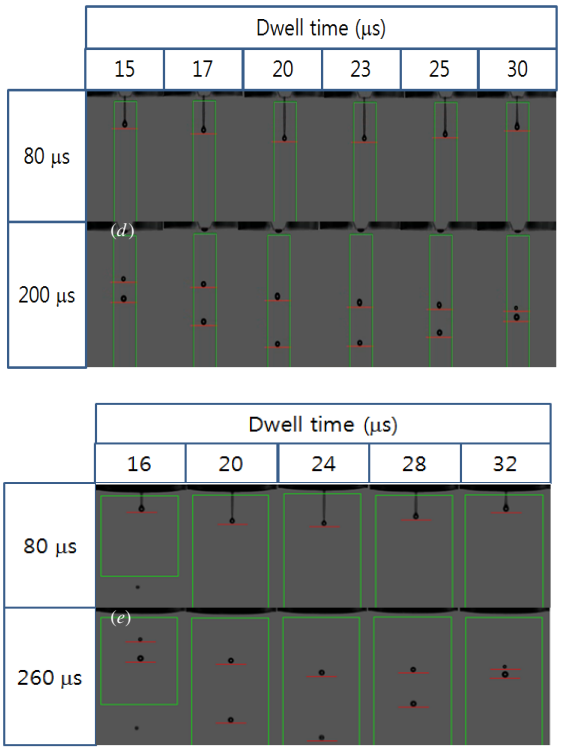


**Figure 8.** (Continued.)

because the speed variation during the drop formation is difficult to measure. Secondly, the conventional method is focused on measuring the jetting speed of the main droplet while neglecting the jetting speed of the satellite. However, the jetting speed of the main droplet alone may not represent the jetting performance in the presence of satellites. If the jetting speed of the satellite is faster, then the faster satellite will add its speed to the jetting speed of the main droplet when the droplets are merged. On the other hand, if the jetting speed of a satellite is slower than the main droplet, the satellite droplet can result in serious placement errors during printing. Therefore, the jetting speed of the satellite should be measured and evaluated in relation to the jetting speed of the main droplet. The proposed instantaneous jetting speed curves can overcome the drawbacks of the conventional method. As seen in figures 9(*c*), (*f*), 10(*c*), (*f*), 11(*c*), (*f*), 12(*c*), (*f*), 13(*c*) and (*f*), the instantaneous jetting speed curves show the jetting speed variation of both the main droplet and satellites during drop formation. Also, the relative jetting speed of satellites with respect to the main droplet can be fully understood during the whole jetting process using the curves.

We observed from the experiment that the jetting speed of the main droplet was fastest in the beginning of jetting when it protruded from the nozzle. Then, the jetting speed of the main droplet was reduced gradually until it became spherical in shape. In contrast, the initial speed of the satellite can even be slightly negative during the breakup process as seen in figures 10(*c*), 11(*c*), 12(*c*) and 13(*c*). The negative jetting speed means that the satellite droplet returns to the nozzle at the time of breakup. This interesting phenomenon seems to

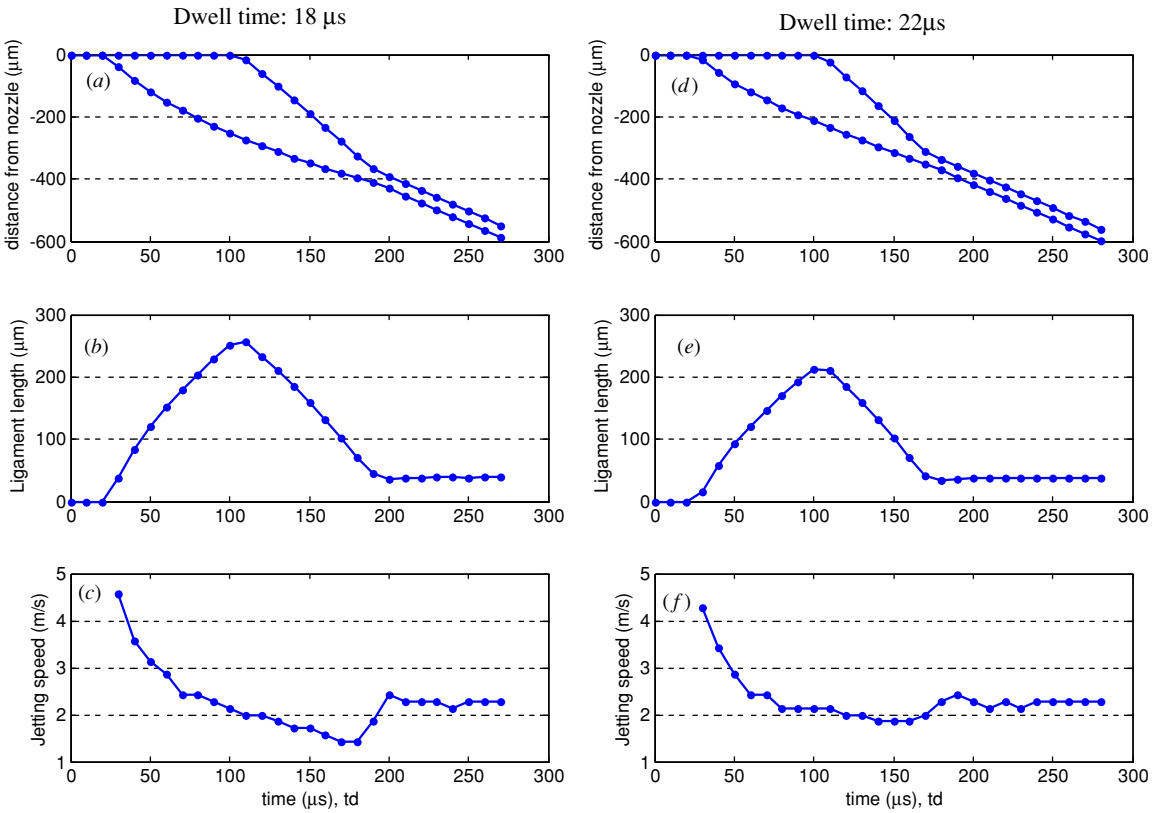


**Figure 9.** Jetting behavior with respect to dwell time (ethylene glycol) (rising/falling time: 6 $\mu$s, 41 V) (*a*), (*d*) DOD drop formation curve; (*b*), (*e*) ligament length; and (*c*), (*f*) instantaneous jetting speed curve.

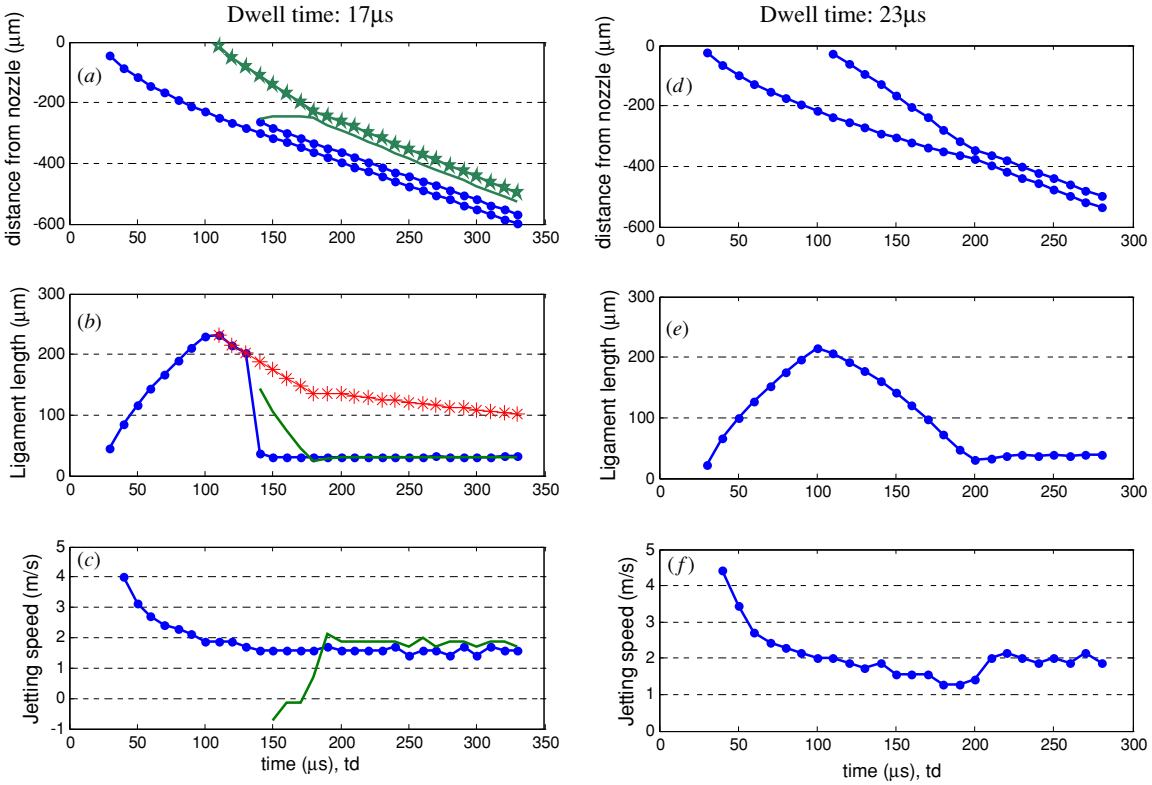


**Figure 10.** Jetting behavior with respect to dwell time (ethylene glycol = 0.75, IPA = 0.25) (rising/falling time: 6 $\mu$s, 34 V). (*a*), (*d*) DOD drop formation curve; (*b*), (*e*) ligament length and (*c*), (*f*) instantaneous jetting speed curve. (—●—: main droplet; ——: satellite; —✳—: equivalent droplet length, $L_{eq}$, —★—: mimimum location of droplets).

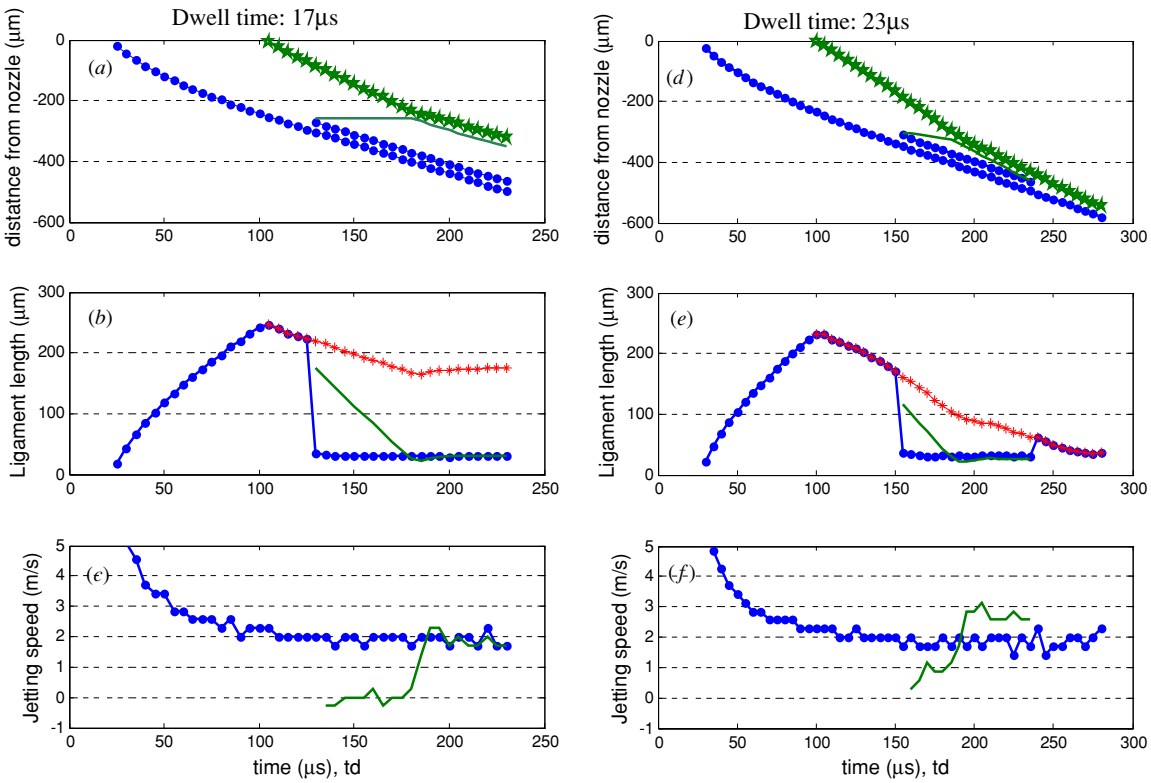


**Figure 11.** Jetting behavior with respect to dwell time (ethylene glycol = 0.5, IPA = 0.5) (rising/falling time: 6 $\mu$s, 32 V). (*a*), (*d*) DOD drop formation curve; (*b*), (*e*) ligament length and (*c*), (*f*) instantaneous jetting speed curve. (—●—: main droplet; ——: satellite; —✳—: equivalent droplet length, $L_{eq}$, —★—: mimimum location of droplets).

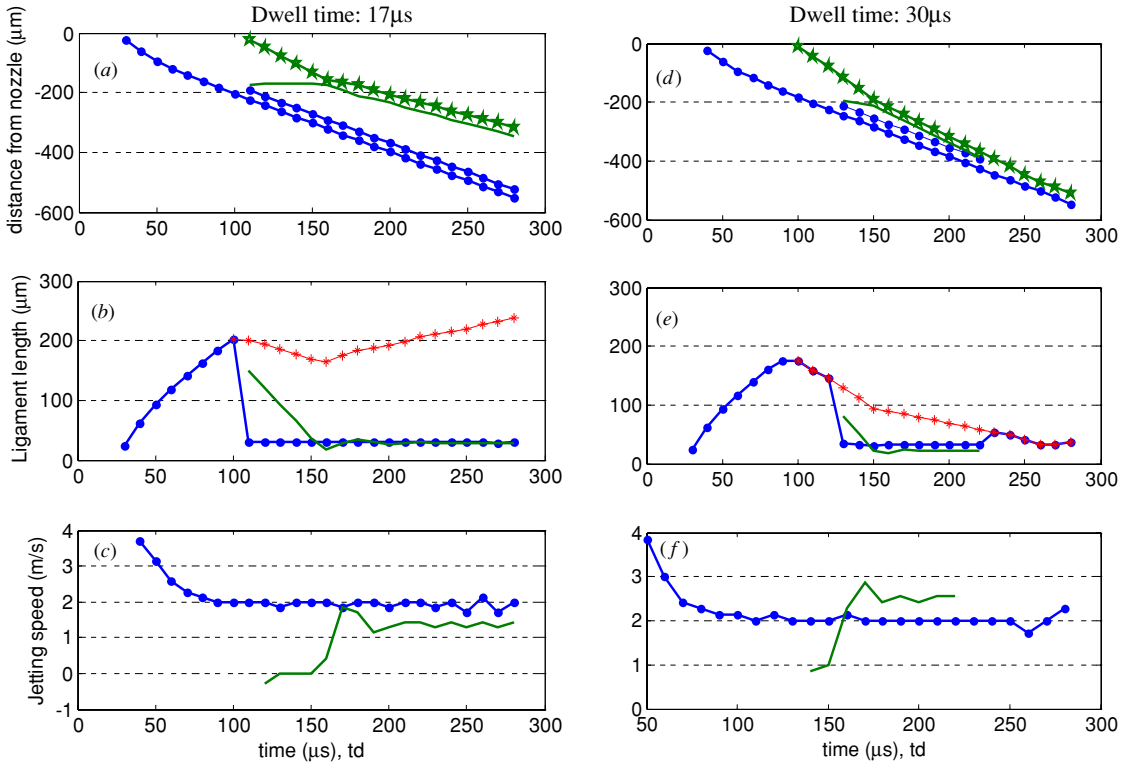


**Figure 12.** Droplet image with respect to dwell time (ethylene glycol = 0.25, IPA = 0.75) (rising/falling time: 6 $\mu$s, 32 V). (*a*), (*d*) DOD drop formation curve; (*b*), (*e*) ligament length and (*c*), (*f*) instantaneous jetting speed curve. (—●—: main droplet; ——: satellite; —✳—: equivalent droplet length, $L_{eq}$, —★—: mimimum location of droplets).

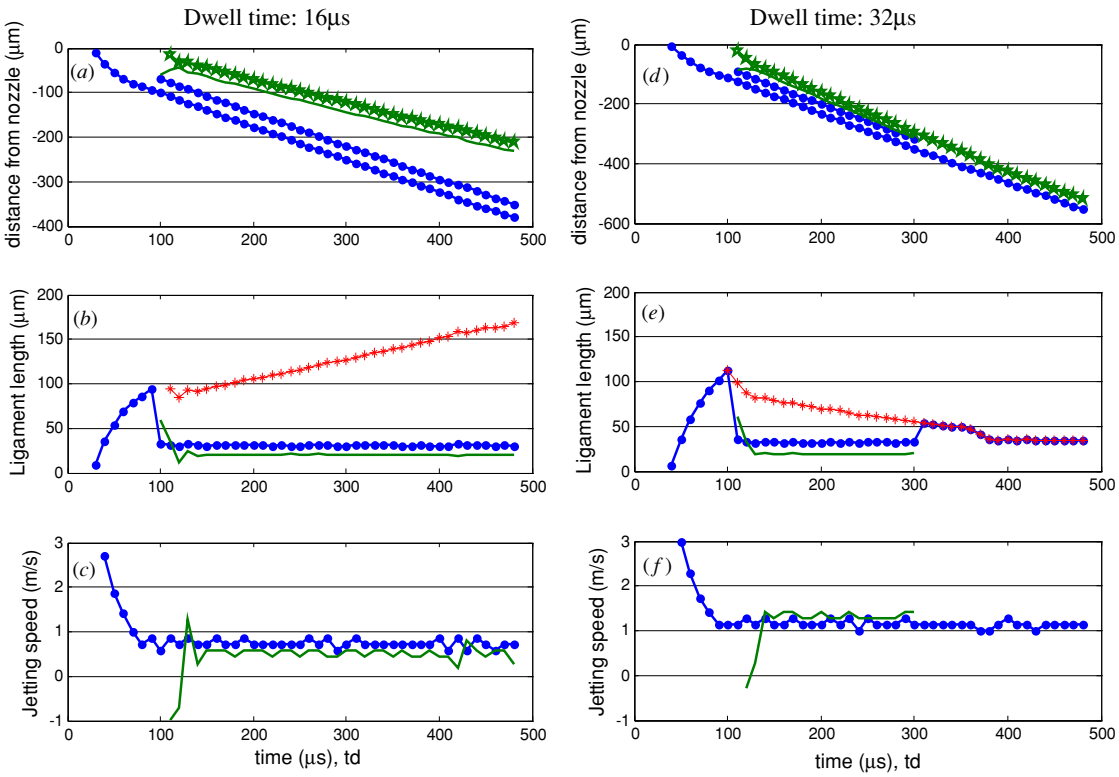


**Figure 13.** Droplet image with respect to dwell time (IPA) (rising/falling time: 6 $\mu$s, 29 V). (*a*), (*d*) DOD drop formation curve; (*b*), (*e*) ligament length; and (*c*), (*f*) instantaneous jetting speed curve. (—●—: main droplet; ——: satellite; —✳—: equivalent droplet length, $L_{eq}$, —★—: mimimum location of droplets).

be related to the elasticity of the fluids and further research is required to understand this behavior fully. We also note that the satellites with lengthy ligaments were likely to remain at low speed (or even negative speed) until they reconciled and become spherical as seen in figures 10(*c*), 11(*c*), 12(*c*) and 13(*c*). After the reconciliation, the satellite speed could be higher than the main droplet as seen in figures 10(*c*) and 12(*f*) or lower than that of the main droplet as seen in figures 12(*c*) and 13(*c*), depending on the jetting fluids and waveform conditions.

### *3.2. Effects of dwell time on drop formation*

Jetting phenomena are related to the pressure wave of ink inside a printhead [14, 15]. However, the pressure wave in ink generated by a waveform voltage is difficult to measure directly. Therefore, in the author's previous works, the self-sensing signal from a piezo was used to measure the pressure wave behaviour in a single nozzle printhead as shown in figure 2, and was compared to meniscus motion [17]. Meniscus motion at the nozzle results from a pressure wave of ink generated from piezo actuation. The meniscus motion in relation to the waveform was measured and discussed in detail in [15]. From [15], the relationship between the dwell time and the pressure wave effect for jetting is illustrated as shown in figure 14 for the inkjet printhead shown in figure 2. The rising and falling sections of the waveform account for pressure wave generation. The dwell time can change the relative phase of the pressure waves generated from the rising and falling sections when the two pressure waves are added for drop ejection. When the positive pressure waves from both the rising and falling sections are in phase, jetting pressure is maximized as shown in figure 14(*b*). The dwell time for the in-phase conditions of the pressure waves has been widely used for controlling inkjet heads [14, 15]. A waveform with the dwell time is referred to as an efficient waveform (or dwell time) since it can maximize the jetting speed of a droplet. On the other hand, the dwell time for 180° out-of-phase pressure waves can result in minimizing the positive pressure waves, and the droplet is not likely to be jetted.

The increase or decrease in dwell time from efficient dwell time will make jetting behavior different due to the two slightly out-of-phase pressure waves generated from the rising and falling sections of the waveform. It has been assumed that the magnitude of pressure wave generated from either the rising or falling section is similar in magnitude except for the sign [15]. Note that the first rising section of the waveform generates a negative pressure wave and it takes some time to reach positive pressure at the nozzle. There is a damping effect during the propagation of the pressure wave. On the other hand, in the case of the falling section, a positive pressure wave for jetting is generated first. So, the positive pressure generated from the falling section is less affected by the damping effect. Thus, the positive pressure generated from the falling section is stronger than the positive pressure from the rising section of the waveform. For example, when the dwell time was shorter than the efficient dwell time, a positive pressure wave from the falling section of the waveform, which

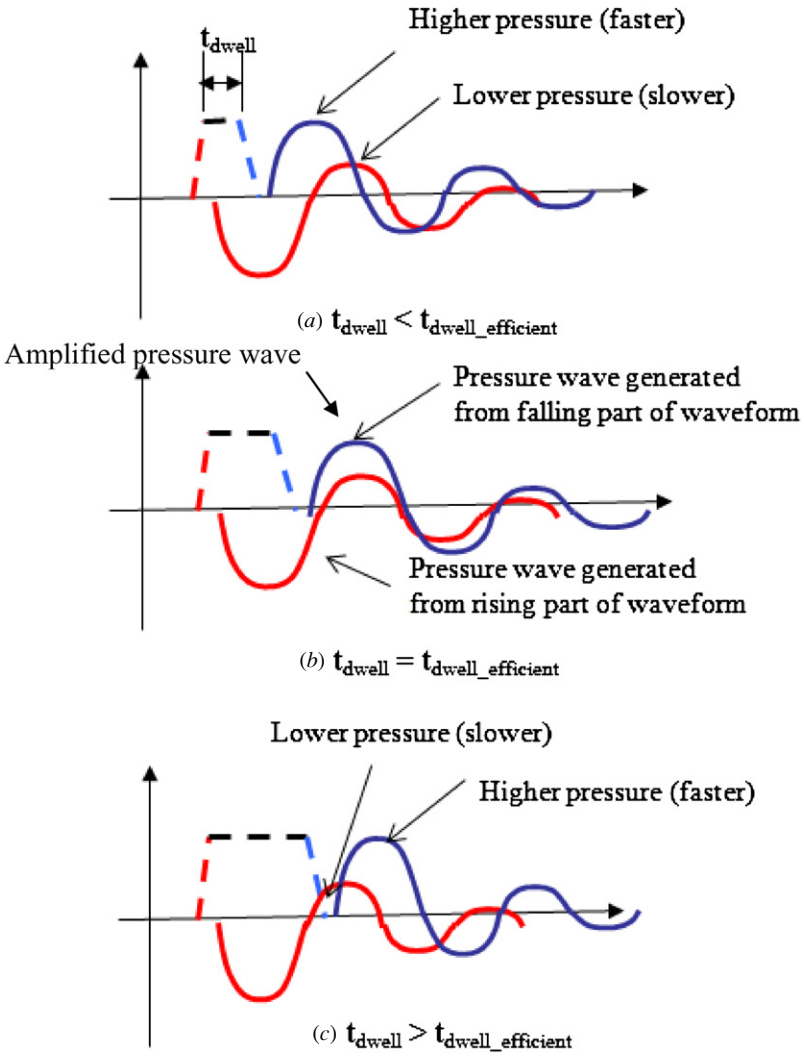


**Figure 14.** Waveform effect on positive wave for jetting.

had strong pressure, came first at the nozzle followed by a weaker positive pressure from the rising time as seen in figure 14(*a*). Thus, the first part of the drop (main drop), which is more strongly influenced by the falling section, is likely to be faster in jetting speed. The latter part of the droplet, which is likely to become a satellite, came later at slow speed due to the weaker pressure wave strength from the rising section. Thus, these two droplets are not likely to merge into a single drop because the later droplet is likely to be slower. For the same reason, the ligament of a droplet tends to be longer.

If the dwell time is slightly longer than the efficient dwell time, then the first part of an extruded droplet can be more influenced by a pressure wave from the rising section as shown in figure 14(*c*). For simplicity, we assumed that two droplets were generated from the waveform shown in figure 14(*c*): the main (or first) drop and the satellite (second) drop. The main droplet was influenced by a weaker positive pressure wave from the rising section, whereas the satellite (second) droplet was influenced by a stronger positive wave from the falling section of the waveform. Thus, the main droplet is likely to be slower than the second satellite droplet. As a result, two drops are likely to merge into one drop. After merging, the first jetted droplet will gain speed since the latter droplet has a faster jetting speed.

Asymmetric jetting speed behavior with respect to dwell time was observed in the dwell time and jetting speed relationship, as shown in figure 7. This is also related to an unbalanced positive pressure wave effect when the positive pressure waves from either the rising section or falling section are slightly out-of-phase.

From the experimental results shown in figures 9–13, it is effective to use a dwell time that is longer than the efficient dwell time to suppress the satellite effect. However, too much deviation from the efficient dwell time may result in no jetting or require increased jetting voltage. Therefore, there is a trade-off between jettability and satellite suppression. For example, in the case of IPA, the satellite effect can be suppressed by using 32 $\mu$s, which is about 30% longer than the efficient dwell time of 24 $\mu$s. However, jetting speed decreased from 2.5 to 1.2 m $s^{-1}$ as shown in figure 7(*e*) by using a dwell time of 32 $\mu$s rather than the efficient dwell time of 24 $\mu$s. Considering the trade-off, we recommend a 20–30% increase

in dwell time from the efficient dwell time to suppress satellite formation. For a better understanding of the effect of dwell time on suppressing satellite behavior, a video can be found on the website cited in [18]. In this study, we considered an inkjet printhead with the simple structure shown in figure 2, where the relationship between the waveform and the pressure wave inside the printhead was straightforward. On the other hand, a commercialized industrial inkjet head could be complicated in structure. The relationship between the waveform and pressure wave might be different from the single nozzle head since the pressure wave reflection might change due to the complicated inkjet head structure. In such a case, the increase in dwell time required to suppress satellites may need to be modified.

### *3.3. Optimal standoff distance*

We demonstrated that jetting behavior could be effectively analyzed using the DOD drop formation curve and instantaneous jetting speed curve. Also we proposed a rule-of-thumb for determining dwell time for suppressing satellites and ligaments. Nonetheless, satellites and ligaments may be unavoidable in some cases. Then, a proper standoff distance (the distance between the inkjet nozzle and substrate) can minimize placement errors due to satellites.

When a ligament or satellite can merge (or reconcile) into a main drop, the standoff distance can be determined to be large enough for droplets to become a spherical single drop. For example, in the case of EG shown in figure 9(*a*), the standoff distance should be larger than 0.4 mm to eliminate placement errors due to length ligament. Here, engineering judgment is required to determine a proper standoff distance since too large standoff distance can result in placement errors due to other causes such as poor jet straightness.

When a satellite did not merge into the main droplet, we define the equivalent droplet length, $L_{eq}(t)$, as a function of time as in equation (3). Then, we evaluate the placement errors and determine a proper standoff distance. Note that if there is a single droplet, the equivalent droplet length is the same as the ligament length of the single droplet. The use of $L_{eq}(t)$ for determining a proper standoff distance is straightforward. For example, as shown in figure 12(*b*), the minimum value for $L_{eq}(t)$ can be found at 160 $\mu$s in figure 12(*b*). Thus, the standoff distance can be determined to be 0.35 mm, which corresponds to the travel distance of the main droplet at 160 $\mu$s (figure 12(*a*)) to minimize placement error due to satellites. Note that the equivalent droplet length can also be used to determine standoff distance when the ligament and satellite merge into the main droplet.

Even though the optimal value for standoff distance can be determined from the equivalent droplet length, we recommended a practical range for a standoff distance to be from 0.3 to 1 mm. A short standoff distance might be considered to be better because it can reduce the possible placement errors from poor jet straightness. However, an insufficient standoff distance may result in mechanical contact between the printhead and substrate unless precise mechanical alignment of the head and substrate is ensured.

## 4. Conclusions

*In situ* techniques to measure jetting behavior were developed such that DOD drop formation and the instantaneous jetting speed curve can be obtained during jetting. Unlike previous inkjet speed measurements using two different timings, the proposed instantaneous jetting speed curve has advantages because the speed variation of droplets during drop formation can be fully understood. From the measured instantaneous jetting speed, the relative jetting speed of the satellite to the main drop was investigated in relation to the dwell time of the driving waveform. From the measured jetting behavior of mixtures of EG and IPA, we recommended a 20–30% longer dwell time with respect to the efficient dwell time to suppress satellite formation. By using a longer dwell time, the ligament length can also be reduced. Also, for unavoidable satellites due to high $Z$ values ($Z > 4$), the longer dwell time resulted in a faster satellite droplet speed. The faster speed was effective in reducing the distance between the satellite and the main droplet. As a result, placement errors due to the satellite can be reduced during printing.

If satellite placement errors are unavoidable, we proposed the use of an equivalent droplet length to determine the optimal standoff distance; thus, satellite effects can be minimized during printing. The optimal standoff distance depends on the relative jetting speed of the satellite drop (the second drop) to the main drop (the first drop). However, engineering judgment is required to determine the standoff distance. A standoff distance that is too short may result in mechanical interference between the head and substrate. If the standoff distance becomes too large, then placement errors due to poor jet straightness can dominate.

## Acknowledgments

The author is grateful to Jung-Kook Go and to Jin-Won Kim for assistance with experiments.

## References

[1] Albertalli D 2005 Gen 7 FPD inkjet equipment development status *SID Symp. Digest of Technical Papers.* vol 36 1200–3
[2] Koo H S, Chen M, Pan P C, Chou L T, Wu F M, Chang S J and Kawai T 2006 Fabrication and chromatic characteristics of the greenish LCD colour-filter layer with nano-particle ink using inkjet printing technique *Display* **27** 124–9
[3] Redinger D, Molesa S, Yin S, Farschi R and Subramanian V 2004 An ink-jet-deposited passive component process for RFID *IEEE Trans. Electron Devices* **51** 1978–83
[4] Calvert P 2001 Inkjet printing for materials and devices *Chem. Mater.* **13** 3299–305
[5] Kwon K S 2009 Speed measurement of ink droplet by using edge detection techniques *Measurement* **42** 44–50
[6] Kipman Y 2009 Three methods of measuring velocity of drops in flight using jetxpert *Proc. NIP25 and Digital Fabrication (Louisville, KY)* pp 71–4
[7] Hutchings I M, Martin G D and Hoath S D 2007 High speed imaging and analysis of jet and drop formation *J. Imaging Sci. Technol.* **51** 438–44
[8] Dong H and Carr W W 2006 An experimental study of drop-on-demand drop formation *Phys. Fluids* **187** 072102

[9] Jang D, Kim D and Moon J 2009 Influence of fluid physical properties on ink-jet printability *Langmuir* **25** 2629–35
[10] Kim M K, Kang H S, Kang K T, Cho Y J, Park M S and Kim Y J 2005 The fluid property dependency on ink jetting characteristics *Proc. 2005 IEEE Int. Conf. on Mechatronics (Taipei, Taiwan)* pp 258–60
[11] Reis N, Ainsley C and Derby B 2005 Ink-jet delivery of particle suspensions by piezoelectric droplet ejectors *J. Appl. Phys.* **97** 094903
[12] Dong H, Carr W W and Morris J F 2006 Visualization of drop-on-demand inkjet: drop formation and deposition *Rev. Sci. Instrum.* **77** 085101
[13] Microfab Technote 1999 Drive waveform effects on ink-jet device performance *Microfab Technote* 99–03
[14] Bogy D B and Talke F E 1984 Experimental and theoretical study of wave propagation phenomena in drop-on-demand ink jet devices *IBM J. Res. Dev.* **28** 314–21
[15] Kwon K S 2009 Waveform design methods for piezo inkjet dispensers based on measured meniscus motion *J. Microelectromech. Syst.* **18** 1118–25
[16] Kim M K, Hwang J Y, Lee S H, Kang K T and Kang H S 2008 Phase matching of pressure wave in a drop-on-demand inkjet printhead *J. Korean Soc. Precis. Eng.* **25** 116–25
[17] Kwon K S 2009 Methods for detecting air bubble in piezo inkjet dispensers *Sensors Actuators* A **153** 50–6
[18] Kwon K S 2010 http://www.youtube.com/watch?v=9_TJ_R_fbTc